Articles in PresS. Am J Physiol Endocrinol Metab (February 24, 2015). doi:10.1152/ajpendo.00562.2014

Skeletal muscle dysfunction is associated with derangements in mitochondrial bioenergetics (but not UCP3) in a rodent model of sepsis

Parjam Zolfaghari[1,3], Jane E Carré[1], Nadeene Parker[3], Nancy A Curtin[2], Michael R Duchen[3], Mervyn Singer[1].

1 Bloomsbury Institute for Intensive Care Medicine, University College London, Cruciform Building, Gower Street, London WC1E 6BT, UK

2 National Heart and Lung Institute, Imperial College London, London, UK

3 Department of Cell and Developmental Biology, University College London, Gower Street, London WC1E 6BT, UK

Corresponding author:

Parjam S Zolfaghari

Current address: Adult Critical Care Unit, 4th Floor, Royal London Hospital, Barts Health NHS Trust, Whitechapel, London E1 1BB

Email: parjam.zolfaghari@bartshealth.nhs.uk

Tel. +44 (0) 7712673051

Authors' details:

Parjam S Zolfaghari

Email: parjam.zolfaghari@bartshealth.nhs.uk

Contribution: Conceived, designed and carried out experiments, analysed data and wrote manuscript

Jane E Carré

Email: J.E.Carre@exeter.ac.uk

Contribution: Designed experiments, analysed data, wrote manuscript

Nadeene Parker

Email: nadeenestewart@gmail.com

Contribution: Designed experiments and analysed data

Nancy Curtin

Email: n.curtin@imperial.ac.uk

Contribution: Designed experiments, provided facilities and analysed data

Michael R Duchen:

Email: m.duchen@ucl.ac.uk

Contribution: Conceived and designed experiments, provided facilities and wrote manuscript

Mervyn Singer

Email: m.singer@ucl.ac.uk

Contribution: Conceived and designed experiments, provided facilities and wrote manuscript

All authors revised and approved final draft.

Abstract:

Muscle dysfunction is a common feature of severe sepsis and multi-organ failure. Recent evidence implicates bioenergetic dysfunction and oxidative damage as important underlying pathophysiological mechanisms. Increased abundance of uncoupling protein-3 (UCP-3) in sepsis suggests increased mitochondrial proton leak, which may reduce mitochondrial coupling efficiency but limit ROS production. Using a murine model, we examined metabolic, cardiovascular and skeletal muscle contractile changes following induction of peritoneal sepsis in *wild-type* and *Ucp3*$^{(-/-)}$ mice. Mitochondrial membrane potential ($\Delta\psi_m$) was measured using two-photon microscopy in living diaphragm, and contractile function was measured in diaphragm muscle strips. The kinetic relationship between membrane potential and oxygen consumption was determined using a modular kinetic approach in isolated mitochondria. Sepsis was associated with significant whole body metabolic suppression, hypothermia and cardiovascular dysfunction. Maximal force generation was reduced and fatigue accelerated in e*x vivo* diaphragm muscle strips from septic mice. Mitochondrial membrane potential was lower in the isolated diaphragm from septic mice despite normal substrate oxidation kinetics and proton leak in skeletal muscle mitochondria. Even though wild-type mice exhibited an absolute 26 ± 6% higher UCP-3 protein abundance at 24 hours, no differences were seen in whole animal or diaphragm physiology, nor in survival rates, between wild-type and *Ucp3*$^{(-/-)}$ mice. In conclusion, this murine sepsis model shows a hypometabolic phenotype with evidence of significant cardiovascular and muscle dysfunction. This was associated with lower $\Delta\psi_m$ and alterations in mitochondrial ATP turnover and phosphorylation pathway. However, UCP-3 does not play an important functional role, despite its upregulation. (246 words)

Keywords: Sepsis, Mitochondria, Metabolism, Uncoupling protein 3, Skeletal muscle

Glossary

i/p	Intraperitoneal
$\Delta\psi_m$	Mitochondrial membrane potential
RER	Respiratory exchange ratio
s/c	Subcutaneous
SDS	Sodium dodecyl sulfate
TMRM	Tetramethylrhodamine methyl ester
TPMP	Methyltriphenylphosphonium
UCP	Uncoupling protein
VO_2	Whole body oxygen consumption
VCO_2	Whole body carbon dioxide production
WT	Wild-type

Introduction

Muscle dysfunction is a common feature of severe sepsis and other critical illnesses, and a major cause of both prolonged intensive care stay (21) and long-term disability (7, 34). Neuropathic and myopathic features are well recognized (7, 38, 40, 50), yet the underlying pathophysiology remains incompletely understood. A net catabolic state, impaired cellular and calcium signalling, bioenergetic dysfunction and oxidative damage are all implicated (30, 33, 50). In both patients and animal models, sepsis is associated with decreased skeletal muscle mitochondrial respiratory capacity, reduced mitochondrial protein levels and increased rates of generation of reactive oxygen and nitrogen species (ROS and RNS) (12, 13, 16, 18, 20, 26), all of which may impair muscle function.

The proton electrochemical gradient created by activity of the mitochondrial respiratory chain generates a transmembrane potential ($\Delta\psi_m$) that is used by the F_oF_1 ATP synthase to phosphorylate ADP to ATP (coupled respiration). However, a variable proportion of protons are uncoupled from ATP synthesis by leaking back into the mitochondrial matrix, the rate of proton flux being dependent upon the magnitude of $\Delta\psi_m$. Proton leak rate is variable and considered to constitute ~20% of the basal metabolic rate of hepatocytes, and up to 50% in rat skeletal muscle (53). Uncoupled respiration has basal and inducible components (35), with the inducible part forming the mechanism of heat generation in brown adipose tissue through uncoupling protein (UCP)-1 (44). Other uncoupling proteins – UCP-2-5 – have been identified but their physiologic role and biochemical mechanisms remain controversial. One suggestion is that following activation by ROS and by-products of ROS damage, these UCPs may induce a mitochondrial proton leak (11, 25) that, in turn, may down-regulate ROS production, forming a negative feedback loop (42).

Processes interfering with maintenance of $\Delta\psi_m$ may impact on cellular energy supply and mitochondrial ROS production (23, 45). Sepsis is associated with high levels of nitric oxide production which impairs respiratory enzyme function (12, 27). Increased expression

of UCP-2 and UCP-3, reported in septic mouse models (60, 66), suggests a possible increase in proton leak with a reduction in mitochondrial coupling efficiency (the proportion of mitochondrial oxygen consumption used to drive ATP synthesis). A consequential decrease in mitochondrial ATP production could have significant impact on muscle contractile function.

The traditional approach of measuring whole body oxygen consumption as a marker of metabolic rate in sepsis does not take into account the proportion of oxygen use that is uncoupled from oxidative phophorylation. This proportion may fluctuate considerably over time, particularly in view of the significant thermoregulatory and inflammatory disturbances that occur in this condition.

The aim of our study was to determine changes in metabolism, muscle function and the influence of UCP3 in an established rodent model of sepsis. We hypothesised that sepsis leads to metabolic suppression and muscle dysfunction as a result of decreased capacity of mitochondrial ATP synthesis, and that UCP3, an uncoupling protein restricted to muscle and adipose tissue, offers protection to ROS-induced muscle contractile dysfunction at the expense of mitochondrial efficiency.

Methods

Mouse septic model. All experiments were performed under the UK Animals (Scientific Procedures) Act 1986 with approval from the University College London Ethics Committee. Ten-week old male C57 black mice were purchased from Charles River (Margate, UK) and maintained in the university animal facility until they reached 25-35 weeks of age. They were housed in cages (maximum 6 per cage) with standard bedding, environment-enhancing objects and free access to water and chow diet. Cages were maintained at room temperature with 12-hour light and dark cycles. Comparison was made against age-matched litter mice from three *Ucp3*$^{(-/-)}$ homozygote breeding pairs (originally produced by Gong *et al* (29) and back-crossed ten generations with wild-type C57 mice). Confirmatory genotyping was carried out using tail snips. All *Ucp3*$^{(-/-)}$ mice were kept in individually ventilated cages with litter-mates of the same sex kept in the same cage after weaning. Mice were allowed to acclimatize to the laboratory for one week prior to the start of experiments.

The model of sepsis has been described in detail elsewhere (67). In summary, sepsis was induced by intraperitoneal injection of diluted cecal slurry (20 ml/kg) under a brief period of isoflurane anesthesia. Sham mice received 20 ml/kg of 0.9% saline i/p. As septic mice stop eating, a further sham starved group was added to account for this potential confounding factor. Starvation commenced after i/p injection of saline. Mice were block-randomized to each treatment group for each set of experiments.

All mice received 0.9% saline 10ml/kg s/c at time 0 h, and 50 ml/kg of 5% dextrose/0.81% saline solution at 6, 18, 30 and 42 h. Initial experiments observed 72-hour survival, serum biochemical markers of organ failure, blood gases and echocardiography (Vivid 7, GE Healthcare, Chalfont St. Giles, Bucks, UK) at 24 hours. Clinical variables comprising behaviour, appearance temperature and acidemia were used to score sepsis severity (67). Severity scoring was carried out by two observers, one of whom was blinded to

the randomization process. The scores given by the two observers were consistently equal. Subsequent studies are outlined below.

Whole animal metabolism. Whole body metabolic rate of sham and septic mice were measured for 24h in individual metabolic chambers (Oxymax, Columbus Instruments, Columbus, OH). Gas samples from each box were sampled for 90 seconds at 8-minute intervals. Oxygen consumption (VO_2) and CO_2 production (VCO_2) were calculated using standard formulae. The respiratory exchange ratio (RER) was calculated as the ratio of VCO_2 to VO_2. Values near 1 indicate a predominance of carbohydrate metabolism while values approaching 0.7 indicate fatty acid oxidation (36). Rectal temperature was measured at 0, 6, 18 and 24h, and animals were weighed at 0 and 24h time-points.

Assessment of cardiac function: Echocardiography was performed at 0, 6 and 24h in sham and septic *wild-type* and *Ucp3*$^{(-/-)}$ mice using a 14 MHz probe connected to a Vivid 7 Dimension device as previously described (67). Aortic blood flow velocity was measured in the proximal ascending aorta immediately before the bifurcation of the right carotid artery using pulse-wave Doppler. Stroke volume was calculated by multiplying the velocity time integral (VTI) from six consecutive cycles (equivalent to one respiratory cycle) by aortic cross-sectional area (using an aortic diameter of 0.26 cm). Average peak-to-peak distance and maximum velocity over six consecutive systolic cycles were used to measure heart rate and peak velocity, the latter being a marker of left ventricular contractility (12). Cardiac output was calculated as the product of stroke volume and heart rate.

Western blotting for UCP3 protein. UCP-3 protein abundance was measured in snap-frozen heart and skeletal muscle tissue at 10 and 24h following induction of sepsis in the *wild-type* mice. After SDS protein precipitation, 10 µg protein was separated on a 12% SDS polyacrylamide gel and transferred to nitrocellulose. Membranes were probed overnight at 4˚C with the primary antibody (Rabbit anti-UCP3: PA1-055 Pierce antibodies, ThermoFisher

Scientific, Loughborough, Leics, UK) at 1:1000 dilutions in blocking buffer. Each sample was loaded twice in the same gel, and each gel repeated once. Following incubation with secondary antibody (goat-anti-rabbit antibody: DAKO, Ely, Cambs, UK), cross-reacted proteins were visualised by enhanced chemiluminescence (Amersham Biosciences, Little Chalfont, Bucks, UK). Densitometry measurements were made using Image J image processing and National Institute of Health analysis software. A single control sample was used in each gel and all results normalized to this control allowing comparison between samples in different gels. Alpha-tubulin (1:5000 dilution, Abcam 7291, Cambridge, Cambs, UK) was used to ensure equal loading of gels and transfer of proteins from gel to membrane. Each membrane was also Coomassie stained to ensure equal loading and transfer.

Diaphragm preparation. At 24h, under terminal isoflurane anesthesia, a midline laparotomy was performed and the diaphragm excised *en-bloc* (still attached to ribs laterally) and pinned (taut without excess stretch) at its edges in a petri dish filled with physiological saline (containing of mmol/L: Na^+ 145, K^+ 5, Ca^{2+} 5, Mg^{2+} 1, HCO_3^- 25, Cl^- 118, SO_4^{2-} 1, PO_4^{3-} 1, glucose 10, pyruvate 10, and equilibrated with 95% O_2 and 5% CO_2 (pH 7.4). Tubocurarine (2.5 μm) was added to stop spontaneous neuromuscular junction activity. Diaphragm strips (~1 mm wide) were dissected using stereomicroscopy; a strip consisted of muscle fibers with the ribs at one end and central tendon at the other. Strips were allowed to rest in physiological saline for at least 30 minutes prior to experimentation. All experiments were performed within 5h of tissue harvest.

Force and power measurements. Aluminium foil T-clips were attached to the rib and central tendon at the ends of the diaphragm strips using cyanoacrylate gel glue. The muscle strips were transferred to a temperature-controlled (23°C) Perspex bath through which physiological saline was continuously circulated. At one end the strip was attached to a combined motor and force transducer (Model 300B, Cambridge Technology, Inc., Watertown, MA, USA) and the other end to a hook mounted onto a micrometer allowing

alteration of resting muscle length. Electrical stimulation (MultiStim System-D330, Digitimer, Welwyn Garden City, Herts, UK) was delivered by two platinum electrodes placed in the bath just above and below the belly of the muscle fibres. A program written in TestPoint (Keithley Instruments, Bracknell, Berks, UK) controlled stimulation and motor arm position and recorded force, length and stimulation. A DAS-1800AO Series A/D board (Keithley Instruments) was used. The computer program could be altered to achieve complex protocols such as force recording during repeated phased cyclical tetanic stimulations while making controlled changes to muscle length.

Following system calibration and zeroing, optimal stimulation voltage (at 96Hz) was found for the muscle strip; these stimulus parameters were used throughout the experiment. The length/tension relationship was explored by increasing the muscle length in 0.2-0.4 mm increments to identify L_0, the muscle length at which filament overlap was optimal for isometric tetanic force development. A single 350 ms tetanic stimulation was used to measure the maximal achievable tetanic isometric force. The maximum force generated was expressed relative to muscle cross-sectional area (CSA) to take account muscle size.

$$CSA = 4.9 \times d \times M / L_0$$

where 4.9 is the wet-to-dry ratio (65), d is density (assumed to be 1 mg/mm^3), M is dry mass of the muscle and L_0 is muscle length as defined above. M and L_0 were measured at the end of the experiment.

The ability of the muscle to produce work and power was measured using a pattern of sinusoidal movement and stimulation that mimics diaphragm muscle action *in vivo.* This pattern was described and optimized by Stevens and Faulkner for diaphragm muscle strips from C57 black mice (59). The amplitude of the length change was ±0.4mm. Stimulation was applied for ~30% of each movement cycle and was approximately centered on the time at

which the muscle length was longest. The maximum power was measured in one cycle of movement at frequency 4Hz. The initial muscle strip length was incrementally increased to find optimal range. To measure the effects of fatigue on power, cycles of length change with stimulation were repeated over a one-minute period. The frequency of movement was 2 Hz, which is equivalent to 120 breaths/min, close to the average respiratory rate measured in septic mice.

The net work performed by the muscle strip is the 'positive work' performed during muscle shortening and contraction, minus the 'negative work' to bring the muscle back to its original length (59). We evaluated net work as follows: Passive force was recorded during movement without electrical stimulation, and then during the same movement with electrical stimulation. The unstimulated record was subtracted from the stimulated record to give the active force value. Net work performed during the movement cycle was evaluated as the area circumscribed by the active force vs. length change graph, referred to as work loop (Fig. 5C). The average power output during the movement cycle was calculated by dividing net work by cycle duration, and is expressed relative to the muscle strip wet weight to take account of size.

Diaphragm muscle mitochondrial membrane potential ($\Delta\psi_m$). Diaphragm muscle strips (3-4 mm wide) taken at 24h from paired fed sham and septic wild-type mice were pinned onto a Sylgard™ imaging chamber and continuously superfused with oxygenated saline solution at 23°C on the stage of an upright epifluorescent microscope (Zeiss Axioskop, Carl Zeiss, Cambridge, Cambs, UK) with a x63 Achroplan water dipping objective and 0.9 numerical aperture. The strips were incubated for 45 min with the lipophilic cationic dye, tetramethylrhodamine methyl ester (TMRM) (Invitrogen, Paisley, Renfrewshire, UK) added to the circulating saline solution at low concentration (100 nM). Fluorophore excitation was achieved using a femtosecond pulsed Ti;sapphire tunable multiphoton laser (Coherent Chameleon, Santa Clara, CA) set at wavelength 720nm. A photomultiplier tube detected the

emitted light, which was first split by a long pass 510nm dichroic mirror before passing through a band pass filter 560-615nm.

Accumulation of TMRM in cells and mitochondria depends on both plasma membrane potential and $\Delta\psi_m$. At low loading concentrations, TMRM fluorescence intensity is linear to its concentration (24). The baseline fluorescence intensity of TMRM in muscle strips isolated from sham and septic mice was measured and directly compared. Fluorescence intensity was also determined in the presence of the ATP synthase inhibitor, oligomycin (10 µg/ml, Sigma-Aldrich, Gillingham, Dorset, UK) and the protonophore, carbonyl cyanide 4-(trifluoromethoxy) phenylhydrazone (FCCP) (1µM, Sigma-Aldrich). The addition of oligomycin can differentiate states where mitochondria are depolarized as a result of high ATP production and flux through the respiratory chain, from other states where a pathological process has resulted in ATP synthase to switch back to its native ATPase activity (17, 28). The addition of FCCP results in dissipation of $\Delta\psi_{m,}$ confirming that the TMRM signal is truly mitochondrial and unquenched.

Stepped z-stacked images (10 at 4µm apart) were taken in all three states (baseline, after oligomycin, after FCCP) and assimilated to form a single projection for measurement of TMRM fluorescence intensity. Three different fields of muscle cells corresponding to the brightest regions of the muscle strip with at least 5 cells per field were analyzed using Zeiss LSM software, and values from the three fields averaged to give a single result per specimen. As it was unclear how $\Delta\psi_m$ would vary between subjects and in sepsis, eight subjects per group were arbitrarily chosen. Statistical comparison was made within the group (i.e. sham or septic) using ANOVA with repeated measures, and between groups using Student's t-test for each state (baseline, +oligomycin, +FCCP).

Isolation of mitochondria from total skeletal muscle. At the 24h time-point, lower limb, back and respiratory skeletal muscle were taken from *wild-type* fed sham, starved sham and septic mice, with clinical severity scoring performed beforehand. Mitochondria were then isolated as described by Bhattacharya *et al* (8) at 4°C. In brief, muscles were rapidly removed, weighed and placed in ice-cold isolation solution (KCl 100mM, Tris/HCl 50mM, EGTA 2mM, pH 7.4 at 4°C). The muscle was minced and the muscle slurry washed and protease-digested in digestion buffer (KCl 100mM, Tris/HCl 50mM, EGTA 2mM, ATP 1mM, $MgCl_2.6H_2O$ 5mM, Defatted Bovine Serum Albumin 0.5%, Protease Type VIII [(245.7units/100ml, Sigma P 5380)], pH 7.4). The mixture was Dounce homogenized and spun for 10 min at 490g. Supernatant was filtered and spun in 2-3 stages for 10 min each at 10,400g. The final pellet (mitochondria) was resuspended in a small volume of isolation medium (0.6-0.8 ml) and protein concentration measured using a BCA protein assay kit (ThermoFisher Scientific).

To determine percentage recovery of mitochondria from skeletal muscle homogenate from all three groups of mice, citrate synthase activity was assayed at each step of the isolation process by spectrophotometric determination of oxaloacetate-dependent coenzyme A-coupled reduction of DTNB at 412nm (57), in an assay adapted for 96-well plates.

Respiratory activity of isolated mitochondria and modular kinetic analysis. Respiratory activity of isolated mitochondria was determined using a Clark electrode chamber (Rank Brothers, Bottisham, Cambs, UK) surrounded by a thermostatically-controlled water jacket at 30°C and calibrated with air-saturated assay medium. Mitochondria (0.35mg/ml) were incubated in assay medium (KCl 120mM, KH_2PO_4 5mM, HEPES 3mM, EGTA 1mM, 0.3% (w/v) de-fatted BSA, pH 7.4).

Respiratory control ratios were calculated as state 3 respiratory rate after addition of ADP (200μM) divided by the state 4 rate after ADP phosphorylation with pyruvate 5mM and malate 2.5mM as substrates. Ratios of 3-10 have been quoted as acceptable RCR ratios (51,

58). FCCP (1-3μM) was added at end-study to measure maximal oxygen consumption rate; a three-fold rise in respiratory rate has been used to indicate good mitochondrial quality (58).

Modular kinetic analysis. This technique allows interrogation of mitochondrial pathways that generate $\Delta\psi_m$ (substrate oxidation), and pathways that utilize/dissipate it (proton leak and ATP turnover) (10, 15, 47, 48). The conceptual division of mitochondrial respiration into these three kinetic modules is further detailed in Figure 1. The modules are divided into a substrate oxidation module ($\Delta\psi_m$ producing); an ATP turnover module, comprising phosphorylation and associated transport activity ($\Delta\psi_m$ dissipating); and a proton leak module ($\Delta\psi_m$ dissipating). Substrate oxidation and proton leak kinetics are determined directly, while ATP turnover is derived by subtracting proton leak from total $\Delta\psi_m$ –dissipating pathway activity. Studies were performed in a specially adapted 7 ml Clark electrode chamber that simultaneously measures oxygen consumption and $\Delta\psi_m$ using a methyltriphenylphosphonium ($TPMP^+$) electrode in the presence of nigericin (0.1μM) to abolish the pH gradient. Following addition of mitochondria (0.35 mg/ml) to the assay medium (KCl 120mM, KH_2PO_4 5mM, HEPES 3mM, EGTA 1mM, 0.3% (w/v) de-fatted BSA, Nigericin 0.1 μM; pH 7.4), the $TPMP^+$ electrode was calibrated with five sequential 0.5 μM additions of TPMP. Mitochondria were energized with succinate 8mM (plus rotenone 5 μM). The starting oxygen level and the zero point were used for two-point calibration of the Clark electrode (100% and 0% points). FCCP was added at the end of all experimental runs to correct for any drift of the $TPMP^+$ electrode. Due to the large number of mitochondria needed for each of the protocols, mitochondria isolated from two mice in the same group were pooled. Each protocol was run twice and the results averaged.

Since the kinetic response of each module to an effector reflects a change in the common intermediate, $\Delta\psi_m$, the kinetic curves of modules that consume protonmotive force are independent of the respiratory substrate used to generate that $\Delta\psi_m$ (2). Succinate (8

mM) was used as a substrate in all experiments, since mitochondrial energization is more readily achieved than with NADH-linked substrates (41). The kinetic dependency of oxygen consumption towards $\Delta\psi_m$ was described for each kinetic pathway module by modulating $\Delta\psi_m$ using effectors targeted towards another module within the system. Substrate oxidation kinetics were measured in the presence of oligomycin (1.3 μM) by sequential depolarization with FCCP (0.2-1 μM). Proton leak kinetics were determined in the presence of oligomycin 1.3 μM by sequential additions of malonate (0.1–2.3 mM). The kinetics of total $\Delta\psi_m$-dissipating activity (proton leak + ATP turnover reactions) were measured under state 3 conditions (ADP 2 mM) by sequential additions of malonate (0.1–2.3 mM). ATP turnover kinetics (phosphorylation and transport reactions) were subsequently calculated by subtraction of proton leak rate from the state 3 respiratory rate at the corresponding value of $\Delta\psi_m$. FCCP (1 μM) was added at the end of all experimental runs to correct for drift of the $TPMP^+$ electrode.

To test for statistical significance, respiration rates between flanking values of $\Delta\psi_m$ were interpolated so that for each curve, oxygen consumption at $\Delta\psi_m$ of -170mV was calculated. This value was the highest $\Delta\psi_m$ common to all conditions. The higher the value of $\Delta\psi_m$, the higher the flux of protons through the various $\Delta\psi_m$-consuming modules, and therefore the more likely to see a result emerging through the inherent noise of the experimental setup. Additionally, uncoupling proteins (UCP3 in particular) may require a high $\Delta\psi_m$ to become active (48). One-way ANOVA was used to test for difference in VO_2 between the groups at $\Delta\psi_m$ of -170mV.

Statistical analysis

Statistical analysis was performed using SPSS 18.0 (IBM) software. Data were normally distributed, unless stated. Student's t-test, Mann-Whitney U tests, and analysis of variance (ANOVA) (with and without repeated measures calculations) were used to test for statistical

significance with the alpha error set to <5% ($p<0.05$). Tukey and Dunnet *post hoc* tests were used to define significance.

Results

Whole body physiology and skeletal muscle function

Mortality and whole-animal metabolism. Mortality rates of the septic wild-type (n=11) and *Ucp3*$^{(-/-)}$ mice (n=12) at 24h, 48h and 72h time-points were similar, at approximately 20%, 70% and 73%, respectively (Figure 2). No deaths occurred in either WT (n=10) or *Ucp3*$^{(-/-)}$ (n=9) sham groups. Septic mice developed a mixed respiratory and metabolic acidosis with biochemical evidence of acute kidney and liver injury (Table 1). The degree of organ dysfunction and acidosis correlated with severity of illness and mortality.

Sepsis produced a large and rapid drop in core temperature and metabolic rate with good correlation between temperature and VO_2 (R^2=0.95) [Fig. 3A-C]. Responses were similar in both wild-type and *Ucp3*$^{(-/-)}$ groups. In both genotypes, the sham fed mice lost a small amount of weight over the first 24 hours (-2 ± 1% SEM body weight change; p=0.08). This was more pronounced in the starved sham mice (-8 ± 1% SEM body weight change; p<0.0001). However, the septic mice gained weight (5 ± 1% SEM body weight; p<0.001), due to a combination of renal dysfunction and fluid sequestration in body cavities (pleural effusions and ascites) and subcutaneous tissues evident at postmortem examination (Fig 3D).

Cardiac function. Echocardiography was performed in 16 sham and 13 severe septic *wild-type* mice, and nine sham and seven severe septic *Ucp3*$^{(-/-)}$ mice (Figure 4). Compared to baseline values, there was a marked reduction in cardiac output at 6 and 24 h in the severe septic mice in both genotypes (p<0.02 within group ANOVA, but no statistical significance between the two genotypes). Decreases were noted in left ventricular contractility

(measured as peak flow velocity), stroke volume and heart rate. No difference was seen between wild-type and *Ucp3*$^{(-/-)}$ groups.

Diaphragm muscle force and power. Measurements were made on diaphragm strips from both wild-type (9 fed sham, 8 starved sham, 9 septic wild-type) and *Ucp3*$^{(-/-)}$ (6 fed sham, 8 starved sham, 7 septic) mice. The average ages (±SEM) were 35±2 weeks for *wild-type* mice and 35±3.5 weeks for *Ucp3*$^{(-/-)}$ mice (p=0.92), with average weights of 32±4 and 34±3 g, respectively (p=0.048). At 24h, maximal tetanic isometric force generated by diaphragm strips from septic wild-type mice was 28% lower than that produced by either fed or starved sham mice ($p<0.05$) (Fig. 5A). Similarly, maximal power generated during a single length cycle at 4 Hz (mimicking 240 breaths/min, typical for normal mice) was 36% and 28% lower in muscle strips from septic mice than from fed and starved sham mice, respectively ($p<0.05$ one-way ANOVA) (Fig. 5B). Similar results were seen in the muscle strips from *Ucp3*$^{(-/-)}$ animals (Figure 5A and B). The work loop profiles generated by all sets of muscle strips showed a similar contraction-relaxation profile (Fig. 5C).

The effect of fatigue on power output was assessed during cycles of movement and stimulation repeated for one minute. A movement frequency of 2 Hz was used to mimic the respiratory rate of 120 breaths/min in a septic mouse. A characteristic pattern of power fatigue was seen: an initial rapid decline was followed by a plateau phase, and then a second rapid decline to a lower plateau (Fig. 5D). The initial power in the fatigue test (Fig. 5D) was about half of the maximum power (shown in Fig. 5B) due to the difference in movement frequency, 2 and 4 Hz respectively. For both genotypes, the power output throughout the fatigue test was lower in the septic group than in either of the sham groups. For both genotypes, the duration of the first plateau ended sooner in the septic group (35 ± 3 cycles) compared to both fed sham (41 ± 6 cycles) and starved sham (41 ± 4 cycles) strips (p= 0.02).

In summary, sepsis resulted in severe hypothermia and metabolic suppression associated with cardiovascular dysfunction, lower muscle force and power generation, and earlier fatigue. As no differences were seen between wild-type and *Ucp3*$^{(-/-)}$mice, this implies that UCP3 does not affect the response to sepsis neither at the level of the whole animal nor at the level of muscle (dys)function. Further experiments were thus performed using only wild-type animals.

Mitochondrial physiology

A detailed analysis of mitochondrial function was performed to determine whether mitochondrial dysfunction, potentially including increased proton leak, could underlie the muscle dysfunction described above. Studies were performed using wild-type mice only.

UCP protein abundance. UCP3 protein expression in diaphragms taken from wild-type sham (n=6) and severe septic mice (n=9) at 24h was assessed by Western blot. UCP3 protein abundance increased by 26±6% (SEM) compared to sham ($p<0.05$). The α-tubulin densitometry signal decreased in septic wild-type mouse diaphragms by 22±7% at 10h [p=0.016], and by 12 ± 6% at 24h [NS]. The ratio of UCP3 to α-tubulin change was 47 ± 13% ($p<0.05$; Figure 6). Coomassie staining confirmed equal protein loading and transfer. UCP2 was not detectable in these samples using 3 different commercially available antibodies.

Mitochondrial membrane potential in diaphragm muscle strips. Muscle strips from nine fed sham and nine septic wild-type mice were compared simultaneously. TMRM loading took 45 minutes to reach steady state prior to imaging. A typical double row and subsarcolemmal high intensity fluorescence pattern was observed in all muscle cells, representing interfibrillar and subsarcolemmal groups of mitochondria (Figures 7A-C). Baseline TMRM fluorescence in diaphragms from *wild-type* septic mice was significantly lower than diaphragms from sham mice, suggesting a decrease in mitochondrial membrane potential ($\Delta\psi_m$) (Figure 7D). The ATP synthase inhibitor, oligomycin was then added to observe

changes in $\Delta\psi_m$ following inhibition of mitochondrial ATP production. This differentiates between states where mitochondria are depolarized as a result of high ATP production and flux through the respiratory chain, from other states where the ATP synthase switches into its native ATPase activity (17, 28). In the diaphragm strips, oligomycin increased TMRM fluorescence, with a greater relative increase above baseline in the septic group (increase of 30 ± 5% in septic diaphragm vs 16 ± 8% in sham; $p<0.001$). Absolute values of fluorescence post-oligomycin were not statistically different between the two groups ($p=0.1$), suggesting the differences are attributable to a difference in proton flux through the F_oF_1-ATPsynthase. The addition of FCCP resulted in complete dissipation of $\Delta\psi_m$ in all specimens examined, confirming unquenched mitochondrial TMRM signal (24).

Citrate synthase activity and respiratory control of isolated mitochondria from skeletal muscle. Mitochondria were isolated from muscles of 8 fed sham, 8 starved sham and 13 severe septic wild-type mice (clinical severity 5-6). Fractional recovery (mean ± SD) of citrate synthase activity at each step of the mitochondrial preparation process compared to the initial muscle homogenate was similar in all three groups, with a final recovery in the mitochondrial pellet of 43 ± 11% (fed sham), 38 ± 23% (starved sham) and 41 ± 9% (septic) ($p=0.48$). The respiratory control of the final mitochondrial pellet measured using the NADH-linked substrates pyruvate and malate was also similar (3.0 ± 0.6 fed sham, 3.5 ± 0.9 starved sham, 2.9 ± 0.5 septic; $p=0.47$).

Modular kinetic analysis of isolated skeletal muscle mitochondria. The effect of sepsis on the kinetic behavior of processes that govern $\Delta\psi_m$ were examined using modular kinetic analysis in 8 fed sham, 8 starved sham and 13 severe septic mice. Substrate oxidation ($\Delta\psi_m$ producing) and proton leak kinetics ($\Delta\psi_m$ consuming) were determined directly, while ATP turnover ($\Delta\psi_m$ consuming) was derived by subtracting proton leak from total $\Delta\psi_m$–dissipating pathway activity. Proton leak kinetics were similar in all three groups (Figs 8 A,B).

455 However, the kinetic behavior of total $\Delta\psi_m$-dissipating processes (Figs 8 C,D) and ATP
456 turnover processes (Figs 8 E,F) were significantly affected in the septic mice: for a given
457 membrane potential (-170 mV), the oxygen consumption rate was significantly lower in
458 mitochondria from septic animals (207 ± 26 fed sham, 157 ± 53 starved sham, 120 ± 30 septic
459 nmol oxygen/min/mg; $p<0.05$). While the substrate oxidation kinetic curves of the septic and
460 fed sham mice were similar (Figs 8 G,H), the curve for the starved sham group (316 ± 19 nmol
461 oxygen/min/mg) was significantly different compared to both fed sham (230 ± 17) and septic
462 (312 ± 22) groups; $p<0.05$), with oxygen consumption rates lower at all values of $\Delta\psi_m$.

463

464 **Discussion**

465 In this rodent model of sepsis and multi-organ failure, we have shown early muscle
466 dysfunction and fatigue associated with metabolic suppression, lower mitochondrial
467 membrane potential and phosphorylation capacity, but no change in mitochondrial proton
468 leak despite an increase in UCP3 protein abundance. These changes were unaffected by
469 presence or absence of UCP3 protein.

470 The pathophysiology of multi-organ failure and muscle dysfunction in established
471 sepsis is complex and multifactorial. Recent interest has focused on bioenergetic
472 dysfunction: increased production of reactive oxygen species results in disruption of
473 metabolic processes and cell damage (12, 13, 61), while decreased transcription of
474 mitochondrial proteins affects respiratory capacity (18, 32). A decrease in cell metabolism
475 may also occur for other reasons, e.g. secondary to a decrease in thyroid activity associated
476 with critical illness (9).

477 Recent publications have highlighted limitations of mouse models of sepsis and the
478 lack of translation of successful treatments from animal models to humans (31, 56). Indeed,

479 significant disparity was reported between mice and humans in their gene expression profile
480 response to inflammatory conditions including sepsis (56). We reported marked differences
481 in the metabolic response to sepsis between rats and mice (67). As seen in the present study,
482 mice showed an early and severity-dependent hypometabolic, hypothermic phenotype with
483 early myocardial depression. This presentation is seen in approximately 10% of cases of
484 human sepsis, and is associated with a 2-3 fold increased risk of mortality (4, 19). However,
485 the ability to define the roles of specific genes by genetic manipulation and to study fully
486 intact biological systems in complex diseases justify an ongoing role for rodent models in
487 defining pathophysiological mechanisms (46). We did make considerable efforts to refine
488 and optimize our murine septic model. These included using older mice equivalent to 30-40
489 year old humans (63), injecting a standardized septic inoculum, providing regular fluid
490 administration to limit hypovolemia-induced tissue hypoperfusion, and performing a block
491 randomization for group allocation in experiments (67).

492 Metabolic suppression and hypothermia are well-described phenomena in septic mice,
493 and are influenced by age, septic insult and ambient temperature (22, 54, 62, 67). We
494 previously demonstrated that rewarming of septic mice to normothermia failed to increase
495 metabolic rate (67), implying a primary metabolic suppression rather than a reactive
496 response to hypothermia.

497 UCP3 is upregulated in sepsis (60, 66), prompting speculation about the role of this
498 protein in decreasing mitochondrial coupling efficiency. This may however act as a negative
499 feedback loop to reduce ROS production (11). We set out to establish the importance and
500 functional consequence of this increase in UCP3 expression, but instead report no detectable
501 differences in the responses of *Ucp3*$^{(-/-)}$ mice to sepsis. Rather than detecting effects on
502 mitochondrial proton leak, our findings suggest that processes related to mitochondrial
503 phosphorylation may be affected.

Previous studies in healthy *Ucp3*$^{(-/-)}$ mice also found little difference in thermoregulation and oxygen consumption rate compared to their wild-type controls (6, 64). Despite a 5-fold increase in skeletal muscle UCP3 in mice given intraperitoneal endotoxin, Yu *et al* in fact described a drop in core temperature to 30°C (66). While we too observed an increase in skeletal muscle UCP3, we found no impact of the lack of UCP-3 protein upon metabolic changes, temperature, cardiovascular and muscle function, or mortality in sepsis. Similarly, while skeletal muscle mitochondria isolated from healthy *Ucp3*$^{(-/-)}$ mice showed more coupled respiration and increased ROS production (64), we could find no differences in force, power and response to repeated stimulation between diaphragm muscle strips isolated from septic wild-type and *Ucp3*$^{(-/-)}$ mice. The original description of the *Ucp3*$^{(-/-)}$ mouse showed no compensatory up-regulation of other UCPs (64), although it is conceivable that such up-regulation may be seen with sepsis. In line with previous work, we were unable to detect UCP2 in muscle from either sham or septic mice using a number of commercially available UCP2 antibodies (data not shown).

We imposed repeated work-loop cycles to mimic *in vivo* diaphragm muscle activity to assess muscle fatigue (59). To our knowledge, the present study is the first description of this functional assessment in a septic model. The plots show a characteristic three-phase response (39); the second phase, a quasi-plateau phase of reduced function, involves recruitment of oxidative metabolism and ends with depletion of high-energy substrates and accumulation of phosphate and other end-products of metabolism (5). We found that this second phase was significantly shorter in septic mice, was affected by hypoxia (data not shown) but was independent of UCP-3 protein expression. This finding supports the notion of linkage between disorders of oxidative metabolism and an inability to maintain high levels of energy substrate.

A significantly lower $\Delta\psi_m$ was seen in the diaphragmatic myocytes of septic mice. While previously shown in cells (1, 55), to our knowledge this is the first demonstration of

altered mitochondrial membrane potential in sepsis in a complex muscle preparation. The low $\Delta\psi_m$ was a consistent finding in the septic mice, and suggests either a decreased rate of $\Delta\psi_m$ generation (e.g. due to a respiratory chain defect) or an increase in turnover of pathways that dissipate the gradient such as proton leak or ATP production (23). Blocking ATP synthase with oligomycin increased fluorescence and hence $\Delta\psi_m$. This rise was significant in the septic group and suggests higher ATP turnover in these diaphragm muscle cells. This was an unexpected finding as previous studies had shown lower respiratory complex activity and lower oxygen consumption in tissues and cells taken from septic animals and humans (13, 16, 20).

Our interrogation of kinetic pathways involved in the maintenance of $\Delta\psi_m$ implies that the mitochondrial pathway that generates $\Delta\psi_m$ through succinate oxidation was unaffected in this model of sepsis. Substrate oxidation rates of mitochondria isolated from starved sham mice were depressed at all values of $\Delta\psi_m$ compared to the other groups. This implies either an altered sensitivity of these mitochondria to FCCP and/or that metabolic adaptations in sepsis do not simply reflect a stressed nutritional state. Previous descriptions of mitochondrial function in sepsis suggest Complex I dysfunction (12, 13). While a full kinetic description of NADH-linked substrate oxidation kinetics was not attempted here due to technical constraints, neither state 3 nor state 4 respiration were significantly different between groups when the mitochondria were energized with complex 1 substrates pyruvate and malate.

Proton leak kinetics were unaffected by the septic insult, despite the rise in UCP3 protein levels in the septic mice, although these experiments were not repeated in the presence of free fatty acids or GDP (47). However, ATP turnover kinetics were significantly affected in the septic mice with lower oxygen consumption rates at given values of $\Delta\psi_m$ when mitochondria were phosphorylating ADP. Defects in ATP synthase in sepsis have been

555 described previously and may explain these observations (16, 37, 43, 52). The higher ATP
556 turnover in the diaphragms of septic mice suggested by the $\Delta\psi_m$ experiments, in conjunction
557 with the altered ATP turnover kinetics seen in muscle mitochondria isolated from septic mice
558 may explain, at least in part, the earlier fatigue observed in the diaphragm muscle strip
559 studies.

560 An issue to consider with the use of isolated mitochondria, especially in conditions
561 such as sepsis, is that removal from their usual cellular environment takes away the impact
562 of local regulatory processes and high levels of inflammatory mediators, and also exposes
563 them to a supranormal oxygen milieu. Such regulatory processes include energy-consuming
564 pathways, resulting in altered ATP demand, or pathways that impose control over substrate
565 trafficking into the mitochondria and substrate oxidation, thereby regulating respiratory
566 chain function and, ultimately, ATP synthesis (14). Nitric oxide, pyruvate dehydrogenase
567 kinase-4 (PDK4) and hypoxia inducible factor-1α (HIF-1α) are all implicated in sepsis (3, 12,
568 49); these likely continue to impose control over mitochondrial function in the intact cell and
569 tissues. Following mitochondrial isolation and washing, and exposure to hyperoxic
570 conditions, such control may be lost. A comparison of our findings using *in situ* and isolated
571 mitochondria implies that sepsis modifies both local regulatory processes and the oxidative
572 phosphorylation machinery itself. These functional changes were not associated with
573 swollen or ruptured mitochondria in an examination of electron micrographs of diaphragm
574 muscles from a limited number of sham and septic mice (data not shown). Although, no
575 formal morphological examination of these were carried out, no gross changes in the shape,
576 size or distribution of mitochondria were noted.

577 In summary, the long-term, resuscitated septic mouse model that we have described
578 exhibits metabolic suppression, hypothermia and decreased cardiovascular activity.
579 Diaphragm muscle strips from septic mice exhibit increased fatiguability *ex vivo;* this may be

related in part to mitochondrial dysfunction. Despite increased UCP3 protein abundance in sepsis, kinetic analysis of isolated mitochondria from skeletal muscle revealed that proton leak kinetics were not different from sham controls, while the lack of UCP3 protein did not impact on mortality, physiological changes or muscle functionality. However, ATP turnover kinetics were significantly altered, implying a defect with ATP synthesis at the level of the F_oF_1 synthase or an associated transport process.

Acknowledgements

We are grateful for the technical help and assistance of Raymond Stidwill and Valerie Taylor with the septic model.

Grants

This work was funded by a MRC Clinical Research Fellowship grant for PSZ.

Disclosures

There are no conflicts of interest to report.

References

1. **Adrie C, Bachelet M, Vayssier-Taussat M, Russo-Marie F, Bouchaert I, Adib-Conquy M, Cavaillon JM, Pinsky MR, Dhainaut JF, and Polla BS.** Mitochondrial membrane potential and apoptosis peripheral blood monocytes in severe human sepsis. *American journal of respiratory and critical care medicine* 164: 389-395, 2001.
2. **Affourtit C, Quinlan CL, and Brand MD.** Measurement of proton leak and electron leak in isolated mitochondria. *Methods in molecular biology (Clifton, NJ)* 810: 165-182, 2012.
3. **Alamdari N, Constantin-Teodosiu D, Murton AJ, Gardiner SM, Bennett T, Layfield R, and Greenhaff PL.** Temporal changes in the involvement of pyruvate dehydrogenase complex in muscle lactate accumulation during lipopolysaccharide infusion in rats. *The Journal of physiology* 586: 1767-1775, 2008.
4. **Arons MM, Wheeler AP, Bernard GR, Christman BW, Russell JA, Schein R, Summer WR, Steinberg KP, Fulkerson W, Wright P, Dupont WD, and Swindell BB.** Effects of ibuprofen on the physiology and survival of hypothermic sepsis. Ibuprofen in Sepsis Study Group. *Critical Care Medicine* 27: 699-707, 1999.
5. **Barclay CJ, Constable JK, and Gibbs CL.** Energetics of fast- and slow-twitch muscles of the mouse. *The Journal of physiology* 472: 61-80, 1993.
6. **Barclay CJ, Woledge RC, and Curtin NA.** Effects of UCP3 genotype, temperature and muscle type on energy turnover of resting mouse skeletal muscle. *Pflügers Archiv : European journal of physiology* 457: 857-864, 2009.
7. **Batt J, dos Santos CC, Cameron JI, and Herridge MS.** Intensive care unit-acquired weakness: clinical phenotypes and molecular mechanisms. *American journal of respiratory and critical care medicine* 187: 238-246, 2013.
8. **Bhattacharya SK, Thakar JH, Johnson PL, and Shanklin DR.** Isolation of skeletal muscle mitochondria from hamsters using an ionic medium containing ethylenediaminetetraacetic acid and nagarse. *Analytical Biochemistry* 192: 344-349, 1991.
9. **Boelen A, Kwakkel J, and Fliers E.** Beyond low plasma T3: local thyroid hormone metabolism during inflammation and infection. *Endocrine reviews* 32: 670-693, 2011.
10. **Brand MD.** The proton leak across the mitochondrial inner membrane. *Biochimica et biophysica acta* 1018: 128-133, 1990.
11. **Brand MD and Esteves TC.** Physiological functions of the mitochondrial uncoupling proteins UCP2 and UCP3. *Cell Metabolism* 2: 85-93, 2005.
12. **Brealey D, Brand M, Hargreaves I, Heales S, Land J, Smolenski R, Davies NA, Cooper CE, and Singer M.** Association between mitochondrial dysfunction and severity and outcome of septic shock. *Lancet* 360: 219-223, 2002.
13. **Brealey D, Karyampudi S, Jacques TS, Novelli M, Stidwill R, Taylor V, Smolenski RT, and Singer M.** Mitochondrial dysfunction in a long-term rodent model of sepsis and organ failure. *American journal of physiology Regulatory, integrative and comparative physiology* 286: R491-497, 2004.

14. **Brown GC.** Control of respiration and ATP synthesis in mammalian mitochondria and cells. *The Biochemical journal* 284 (Pt 1): 1-13, 1992.
15. **Brown GC and Cooper CE.** *Bioenergetics: A practical approach*: IRL Press, 1995.
16. **Callahan LA and Supinski GS.** Sepsis induces diaphragm electron transport chain dysfunction and protein depletion. *American journal of respiratory and critical care medicine* 172: 861-868, 2005.
17. **Campanella M, Parker N, Tan CH, Hall AM, and Duchen MR.** IF(1): setting the pace of the F(1)F(o)-ATP synthase. *Trends in biochemical sciences* 34: 343-350, 2009.
18. **Carré JE, Orban J-C, Re L, Felsmann K, Iffert W, Bauer M, Suliman HB, Piantadosi CA, Mayhew TM, Breen P, Stotz M, and Singer M.** Survival in critical illness is associated with early activation of mitochondrial biogenesis. *American journal of respiratory and critical care medicine* 182: 745-751, 2010.
19. **Clemmer TP, Fisher CJ, Bone RC, Slotman GJ, Metz CA, and Thomas FO.** Hypothermia in the sepsis syndrome and clinical outcome. The Methylprednisolone Severe Sepsis Study Group. *Critical Care Medicine* 20: 1395-1401, 1992.
20. **Crouser ED, Julian MW, Blaho DV, and Pfeiffer DR.** Endotoxin-induced mitochondrial damage correlates with impaired respiratory activity. *Critical Care Medicine* 30: 276-284, 2002.
21. **De Jonghe B, Sharshar T, Lefaucheur J-P, Authier F-J, Durand-Zaleski I, Boussarsar M, Cerf C, Renaud E, Mesrati F, Carlet J, Raphaël J-C, Outin H, Bastuji-Garin S, and Réanimation GdRedaEdNe.** Paresis acquired in the intensive care unit: a prospective multicenter study. *JAMA : the journal of the American Medical Association* 288: 2859-2867, 2002.
22. **Dogan MD, Ataoglu H, and Akarsu ES.** Effects of different serotypes of Escherichia coli lipopolysaccharides on body temperature in rats. *Life sciences* 67: 2319-2329, 2000.
23. **Duchen MR.** Mitochondria in health and disease: perspectives on a new mitochondrial biology. *Molecular aspects of medicine* 25: 365-451, 2004.
24. **Duchen MR, Surin A, and Jacobson J.** Imaging mitochondrial function in intact cells. *Methods in enzymology* 361: 353-389, 2003.
25. **Echtay KS, Roussel D, St-Pierre J, Jekabsons MB, Cadenas S, Stuart JA, Harper JA, Roebuck SJ, Morrison A, Pickering S, Clapham JC, and Brand MD.** Superoxide activates mitochondrial uncoupling proteins. *Nature* 415: 96-99, 2002.
26. **Fredriksson K, Hammarqvist F, Strigård K, Hultenby K, Ljungqvist O, Wernerman J, and Rooyackers O.** Derangements in mitochondrial metabolism in intercostal and leg muscle of critically ill patients with sepsis-induced multiple organ failure. *American journal of physiology Endocrinology and metabolism* 291: E1044-1050, 2006.
27. **Frost MT, Wang Q, Moncada S, and Singer M.** Hypoxia accelerates nitric oxide-dependent inhibition of mitochondrial complex I in activated macrophages. *American journal of physiology Regulatory, integrative and comparative physiology* 288: R394-400, 2005.
28. **Garedew A, Henderson SO, and Moncada S.** Activated macrophages utilize glycolytic ATP to maintain mitochondrial membrane potential and prevent apoptotic cell death. *Cell Death and Differentiation* 17: 1540-1550, 2010.

29. **Gong DW, Monemdjou S, Gavrilova O, Leon LR, Marcus-Samuels B, Chou CJ, Everett C, Kozak LP, Li C, Deng C, Harper ME, and Reitman ML.** Lack of obesity and normal response to fasting and thyroid hormone in mice lacking uncoupling protein-3. *The Journal of biological chemistry* 275: 16251-16257, 2000.
30. **Griffiths RD and Hall JB.** Intensive care unit-acquired weakness. *Critical Care Medicine* 38: 779-787, 2010.
31. **Hackam DG and Redelmeier DA.** Translation of research evidence from animals to humans. *JAMA : the journal of the American Medical Association* 296: 1731-1732, 2006.
32. **Haden DW, Suliman HB, Carraway MS, Welty-Wolf KE, Ali AS, Shitara H, Yonekawa H, and Piantadosi CA.** Mitochondrial biogenesis restores oxidative metabolism during Staphylococcus aureus sepsis. *American journal of respiratory and critical care medicine* 176: 768-777, 2007.
33. **Hermans G, De Jonghe B, Bruyninckx F, and Van den Berghe G.** Clinical review: Critical illness polyneuropathy and myopathy. *Critical care (London, England)* 12: 238, 2008.
34. **Iwashyna TJ, Ely EW, Smith DM, and Langa KM.** Long-term cognitive impairment and functional disability among survivors of severe sepsis. *JAMA : the journal of the American Medical Association* 304: 1787-1794, 2010.
35. **Jastroch M, Divakaruni AS, Mookerjee S, Treberg JR, and Brand MD.** Mitochondrial proton and electron leaks. *Essays in Biochemistry* 47: 53-67, 2010.
36. **Jéquier E, Acheson K, and Schutz Y.** Assessment of energy expenditure and fuel utilization in man. *Annual review of nutrition* 7: 187-208, 1987.
37. **Kantrow SP, Taylor DE, Carraway MS, and Piantadosi CA.** Oxidative metabolism in rat hepatocytes and mitochondria during sepsis. *Archives of biochemistry and biophysics* 345: 278-288, 1997.
38. **Kress JP and Hall JB.** ICU-acquired weakness and recovery from critical illness. *The New England journal of medicine* 370: 1626-1635, 2014.
39. **Lännergren J and Westerblad H.** Force decline due to fatigue and intracellular acidification in isolated fibres from mouse skeletal muscle. *The Journal of physiology* 434: 307-322, 1991.
40. **Latronico N and Bolton CF.** Critical illness polyneuropathy and myopathy: a major cause of muscle weakness and paralysis. *The Lancet Neurology* 10: 931-941, 2011.
41. **Lionetti L, Iossa S, Brand MD, and Liverini G.** Relationship between membrane potential and respiration rate in isolated liver mitochondria from rats fed an energy dense diet. *Molecular and cellular biochemistry* 158: 133-138, 1996.
42. **Mailloux RJ and Harper M-E.** Mitochondrial proticity and ROS signaling: lessons from the uncoupling proteins. *Trends in endocrinology and metabolism: TEM* 23: 451-458, 2012.
43. **Mela L, Bacalzo LV, and Miller LD.** Defective oxidative metabolism of rat liver mitochondria in hemorrhagic and endotoxin shock. *The American journal of physiology* 220: 571-577, 1971.
44. **Nicholls DG.** A history of UCP1. *Biochemical Society transactions* 29: 751-755, 2001.
45. **Nicholls DG and Ferguson SJ.** *Bioenergetics (Third Edition)*, 2002.
46. **Osuchowski MF, Remick DG, Lederer JA, Lang CH, Aasen AO, Aibiki M, Azevedo LC, Bahrami S, Boros M, Cooney R, Cuzzocrea S, Jiang Y, Junger WG,**

Hirasawa H, Hotchkiss RS, Li X-A, Radermacher P, Redl H, Salomao R, Soebandrio A, Thiemermann C, Vincent J-L, Ward P, Yao Y-M, Yu H-P, Zingarelli B, and Chaudry IH. Abandon the mouse research ship? Not just yet! *Shock (Augusta, Ga)* 41: 463-475, 2014.

47. **Parker N, Affourtit C, Vidal-Puig A, and Brand MD.** Energization-dependent endogenous activation of proton conductance in skeletal muscle mitochondria. *The Biochemical journal* 412: 131-139, 2008.

48. **Parker N, Vidal-Puig A, and Brand MD.** Stimulation of mitochondrial proton conductance by hydroxynonenal requires a high membrane potential. *Bioscience reports* 28: 83-88, 2008.

49. **Peyssonnaux C, Cejudo-Martin P, Doedens A, Zinkernagel AS, Johnson RS, and Nizet V.** Cutting edge: Essential role of hypoxia inducible factor-1alpha in development of lipopolysaccharide-induced sepsis. *Journal of immunology (Baltimore, Md : 1950)* 178: 7516-7519, 2007.

50. **Puthucheary Z, Harridge S, and Hart N.** Skeletal muscle dysfunction in critical care: wasting, weakness, and rehabilitation strategies. *Critical Care Medicine* 38: S676-682, 2010.

51. **Rasmussen HN and Rasmussen UF.** Small scale preparation of skeletal muscle mitochondria, criteria of integrity, and assays with reference to tissue function. *Molecular and cellular biochemistry* 174: 55-60, 1997.

52. **Robichaud S, Lalu M, Udenberg T, Schulz R, and Sawicki G.** Proteomics analysis of changes in myocardial proteins during endotoxemia. *Journal of Proteomics* 72: 648-655, 2009.

53. **Rolfe DF and Brown GC.** Cellular energy utilization and molecular origin of standard metabolic rate in mammals. *Physiological reviews* 77: 731-758, 1997.

54. **Rudaya AY, Steiner AA, Robbins JR, Dragic AS, and Romanovsky AA.** Thermoregulatory responses to lipopolysaccharide in the mouse: dependence on the dose and ambient temperature. *American journal of physiology Regulatory, integrative and comparative physiology* 289: R1244-1252, 2005.

55. **Růzicka M, Skobisová E, Dlasková A, Santorová J, Smolková K, Spacek T, Zácková M, Modrianský M, and Jezek P.** Recruitment of mitochondrial uncoupling protein UCP2 after lipopolysaccharide induction. *The international journal of biochemistry & cell biology* 37: 809-821, 2005.

56. **Seok J, Warren HS, Cuenca AG, Mindrinos MN, Baker HV, Xu W, Richards DR, McDonald-Smith GP, Gao H, Hennessy L, Finnerty CC, López CM, Honari S, Moore EE, Minei JP, Cuschieri J, Bankey PE, Johnson JL, Sperry J, Nathens AB, Billiar TR, West MA, Jeschke MG, Klein MB, Gamelli RL, Gibran NS, Brownstein BH, Miller-Graziano C, Calvano SE, Mason PH, Cobb JP, Rahme LG, Lowry SF, Maier RV, Moldawer LL, Herndon DN, Davis RW, Xiao W, Tompkins RG, and the Inflammation and Host Response to Injury LSCRP.** Genomic responses in mouse models poorly mimic human inflammatory diseases. *Proceedings of the National Academy of Sciences of the United States of America*, 2013.

57. **Srere PA.** The citrate enzymes: their structures, mechanisms, and biological functions. *Current topics in cellular regulation* 5: 229-283, 1972.

58. **St-Pierre J, Buckingham JA, Roebuck SJ, and Brand MD.** Topology of superoxide production from different sites in the mitochondrial electron transport chain. *The Journal of biological chemistry* 277: 44784-44790, 2002.

59. **Stevens ED and Faulkner JA.** The capacity of mdx mouse diaphragm muscle to do oscillatory work. *The Journal of physiology* 522 Pt 3: 457-466, 2000.
60. **Sun X, Wray C, Tian X, Hasselgren P-O, and Lu J.** Expression of uncoupling protein 3 is upregulated in skeletal muscle during sepsis. *American journal of physiology Endocrinology and metabolism* 285: E512-520, 2003.
61. **Supinski GS and Callahan LA.** Free radical-mediated skeletal muscle dysfunction in inflammatory conditions. *Journal of applied physiology (Bethesda, Md : 1985)* 102: 2056-2063, 2007.
62. **Tateda K, Matsumoto T, Miyazaki S, and Yamaguchi K.** Lipopolysaccharide-induced lethality and cytokine production in aged mice. *Infection and immunity* 64: 769-774, 1996.
63. **Turnbull IR, Wlzorek JJ, Osborne D, Hotchkiss RS, Coopersmith CM, and Buchman TG.** Effects of age on mortality and antibiotic efficacy in cecal ligation and puncture. *Shock (Augusta, Ga)* 19: 310-313, 2003.
64. **Vidal-Puig AJ, Grujic D, Zhang CY, Hagen T, Boss O, Ido Y, Szczepanik A, Wade J, Mootha V, Cortright R, Muoio DM, and Lowell BB.** Energy metabolism in uncoupling protein 3 gene knockout mice. *The Journal of biological chemistry* 275: 16258-16266, 2000.
65. **Woledge RC and Curtin NA.** The efficiency of energy conversion by swimming muscles of fish. *Advances in experimental medicine and biology* 332: 735-743; discussion 744-737, 1993.
66. **Yu XX, Barger JL, Boyer BB, Brand MD, Pan G, and Adams SH.** Impact of endotoxin on UCP homolog mRNA abundance, thermoregulation, and mitochondrial proton leak kinetics. *American journal of physiology Endocrinology and metabolism* 279: E433-446, 2000.
67. **Zolfaghari PS, Pinto BB, Dyson A, and Singer M.** The metabolic phenotype of rodent sepsis: cause for concern. *Intensive Care Med Exp in press OpenURL*, 2013.

Figure legends

Figure 1 Simplified illustration of mitochondrial bioenergetic pathways split into three groups of reactions: 1) reactions that generate $\Delta\psi_m$ (substrate kinetics), 2) reactions consuming $\Delta\psi_m$ to generate ATP (phosphorylation kinetics), and 3) reactions that consume $\Delta\psi_m$ without generating ATP (leak kinetics). Adapted from Nicholls & Ferguson 2002.

Figure 2 Survival curve of wild-type (n=11) and UCP3$^{(-/-)}$ mice (n=12) after i/p injection of fecal slurry. Sham mice (10 wild-type, 9 UCP3$^{(-/-)}$) received i/p saline. All animals received s/c fluids at 0, 6, 18, 30 and 42 hour time-points.

Figure 3 Temperature (A) and oxygen consumption (B) of wild-type and UCP3$^{(-/-)}$ mice following induction of sepsis (or sham controls). (C) Plot of oxygen consumption against core temperature of wild-type and UCP3$^{(-/-)}$ mice. Line of best fit and correlation coefficient are noted on the graph. (D) Percentage weight change of sham and septic mice over 24 hours. Statistical significance ($p<0.05$) was seen between groups in each genotype. All mice received s/c fluid at 0, 6 and 18h time-points; food was withdrawn from starved sham mice immediately after i/p injection of saline.

* $p<0.05$ compared to fed sham using two-way ANOVA for temperature data over time, and one-way ANOVA for weight data.

Figure 4 Echocardiography results of wild-type and *Ucp3*$^{(-/-)}$ mice following i/p injection of fecal slurry or n-saline. All septic mice were in the severe category according to the clinical scoring scale. Results are mean ± SEM. *$p<0.02$ comparing sham values between the two genotypes; § $p<0.01$ comparing septic and sham values in same genotype using two-way ANOVA repeated measures.

845

846 **Figure 5** (A) Maximal isometric force generated by 350ms tetanic stimulation in diaphragm
847 strips taken from wild-type and *Ucp3*$^{(-/-)}$ mice and normalized to cross-sectional area. (B)
848 Power generated by the muscle strips during sinusoidal length change at 4Hz with phasic
849 tetanic stimulation simulating *in vivo* muscle function. Power is expressed relative to muscle
850 wet weight. (C) Example of a work-loop generated by muscle strips from WT fed sham,
851 starved sham and septic mice (optimal muscle lengths: 8.4mm, 9.5mm, 9.7mm; muscle dry
852 weight: 0.665mg, 0.627mg, 0.578mg, respectively). (D) Power performance of diaphragm
853 strips taken from fed sham and septic wild-type and *Ucp3*$^{(-/-)}$ mice undertaking 120 repeated
854 work-loop cycles at 2Hz over a 1 minute period. Values are the average power per cycle; for
855 clarity some values are not shown. The initial rapid decline is shallower, and the first plateau
856 ends earlier (marked by broken vertical line), in the septic groups in both genotypes
857 compared to the sham group. Values are mean ± 1 SEM.

858

859 **Figure 6** Representative Western blots of UCP-3 protein content of diaphragm muscles from
860 sham (n=6) and septic wild-type mice 24 h after injection of fecal slurry (n=8). B Mean (±SD)
861 densitometry values of UCP-3 protein abundance at 10 h and 24 h in diaphragm muscle.
862 Values were normalized to alpha-tubulin content. * $p<0.05$ compared to sham using one-way
863 ANOVA.

864

865 **Figure 7** Live-cell images of TMRM (A) and Mitotracker green (B&C) fluorescence pattern in
866 diaphragm muscle cells. Two distinct mitochondrial subpopulation of subsarcolemmal (SS)
867 and intefibrillar (IF) are seen. Characteristic double band pattern of interfibrillar
868 mitochondria is shown in B (arrowed). (C) Z-stack 3-D image projection of a diaphragm strip
869 loaded with Mitotracker Green showing muscle and pleural cells on the surface. (D) Average

870 TMRM fluorescence intensity of isolated diaphragms strips from sham and septic *wild-type*
871 mice at 24h bathed in TMRM 100nM (baseline), and after addition of oligomycin 5 μg/ml.
872 (*p=0.016 independent sample t-test; § p<0.01 paired sample t-test comparing oligomycin to
873 baseline fluorescence in the septic group).

874

875 **Figure 8** Dependency of oxygen consumption rate on $\Delta\psi_m$ for different $\Delta\psi_m$–producing and -
876 dissipating kinetic modules (left panels), with oxygen consumption rates at $\Delta\psi_m$ of -170mV
877 (right panels), for mitochondria isolated from total skeletal muscle of septic, fed sham and
878 fasted sham mice. A & B, proton leak kinetics; C & D, total $\Delta\psi_m$–dissipating pathways (proton
879 leak + ATP turnover reactions) under state 3 conditions; E & F; ATP turnover kinetics
880 (phosphorylation + transport reactions) – kinetic curves derived from subtraction of A from
881 C; G & H, substrate (succinate) oxidation kinetics.

882 *p<0.05 one-way ANOVA significance of septic vs. both sham groups; ** p<0.05 one-way
883 ANOVA starved sham vs. fed sham and septic groups.

884

885

886

887 **Table 1** Blood gas and serum biochemistry at 24 hours in *wild-type* mice following

888 induction of sepsis with comparison against sham controls.

	pH	**pCO_2** kPa	**pO_2** kPa	**Lactate** mmol/l	**Hb** g/dl	**Glucose** mmol/L	**Urea** mmol/l	**Creatinine** µmol/l	**AST** IU/l	**ALT** IU/l
Sham	7.33 ± 0.03	4.3 ± 0.3	13.4 ± 4.2	2.4 ± 0.9	13.2 ± 0.2	11.7 ± 4.0	6.5 ± 2.0	10 ± 6	61 ± 30	24 ± 14
Septic	6.96 ± 0.12*	8.5 ± 4.1*	12.2 ± 4.3	5.0 ± 1.2*	15.1 ± 1.6*	14.9 ± 2.4*	34 ± 28*	30±15*	266 ± 95*	77 ± 28*

889 (mean ± SD *p<0.05)

890 Hb Hemoglobin, AST Aspartate transaminase, ALT Alanine aminotransferase, IU international unit.

891

Figure 1

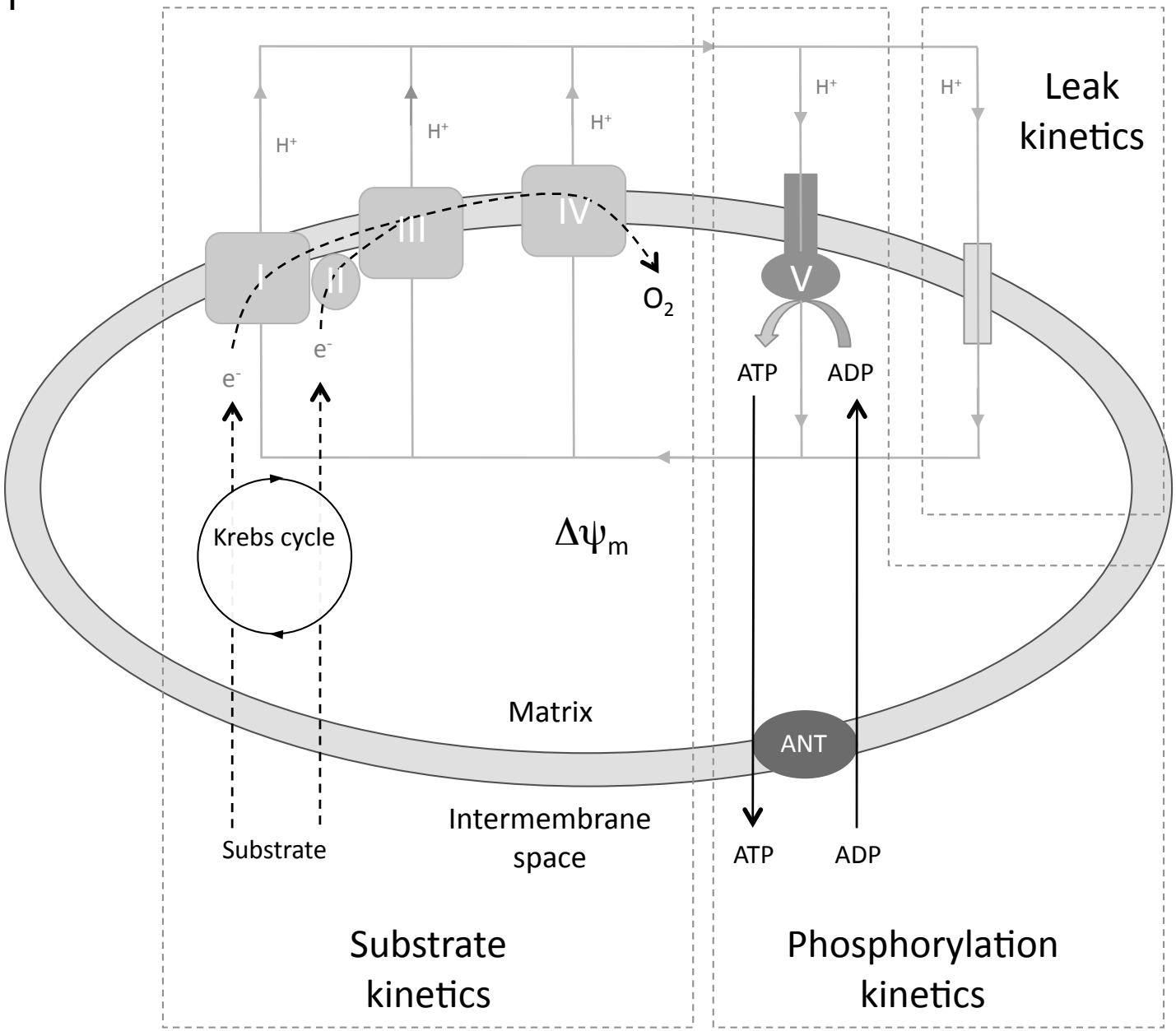
H+
H+
H+
H+
H+
Leak
kinetics
I
II
III
IV
V
O2
e-
e-
ATP
ADP
Krebs cycle
Δψm
Matrix
ANT
Intermembrane
space
Substrate
ATP
ADP
Substrate
kinetics
Phosphorylation
kinetics

Figure 2

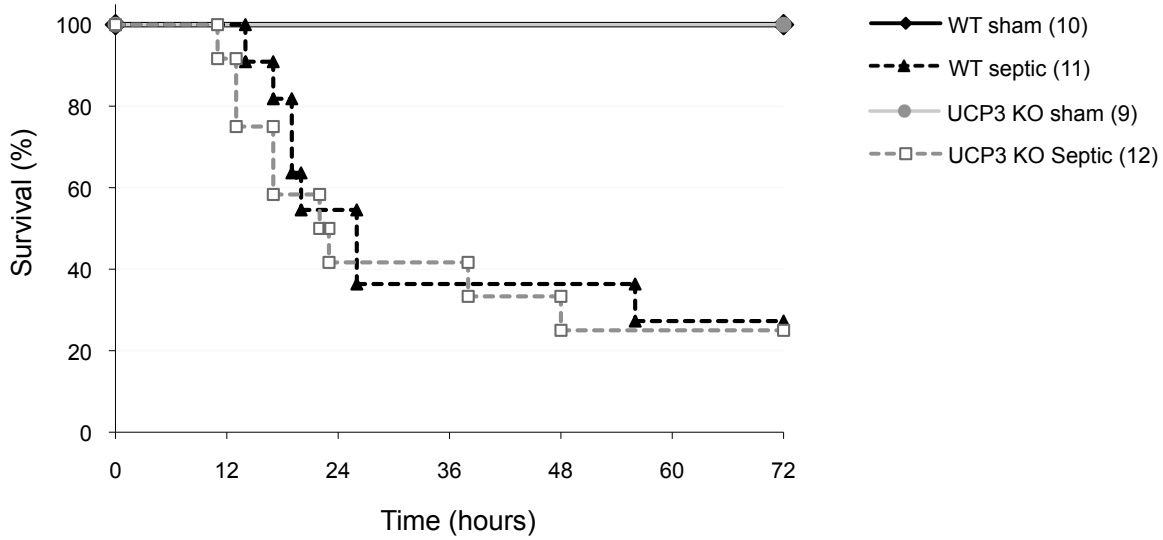
100
80
60
40
20
0
Survival (%)
0
12
24
36
48
60
72
Time (hours)
WT sham (10)
WT septic (11)
UCP3 KO sham (9)
UCP3 KO Septic (12)

Figure 3

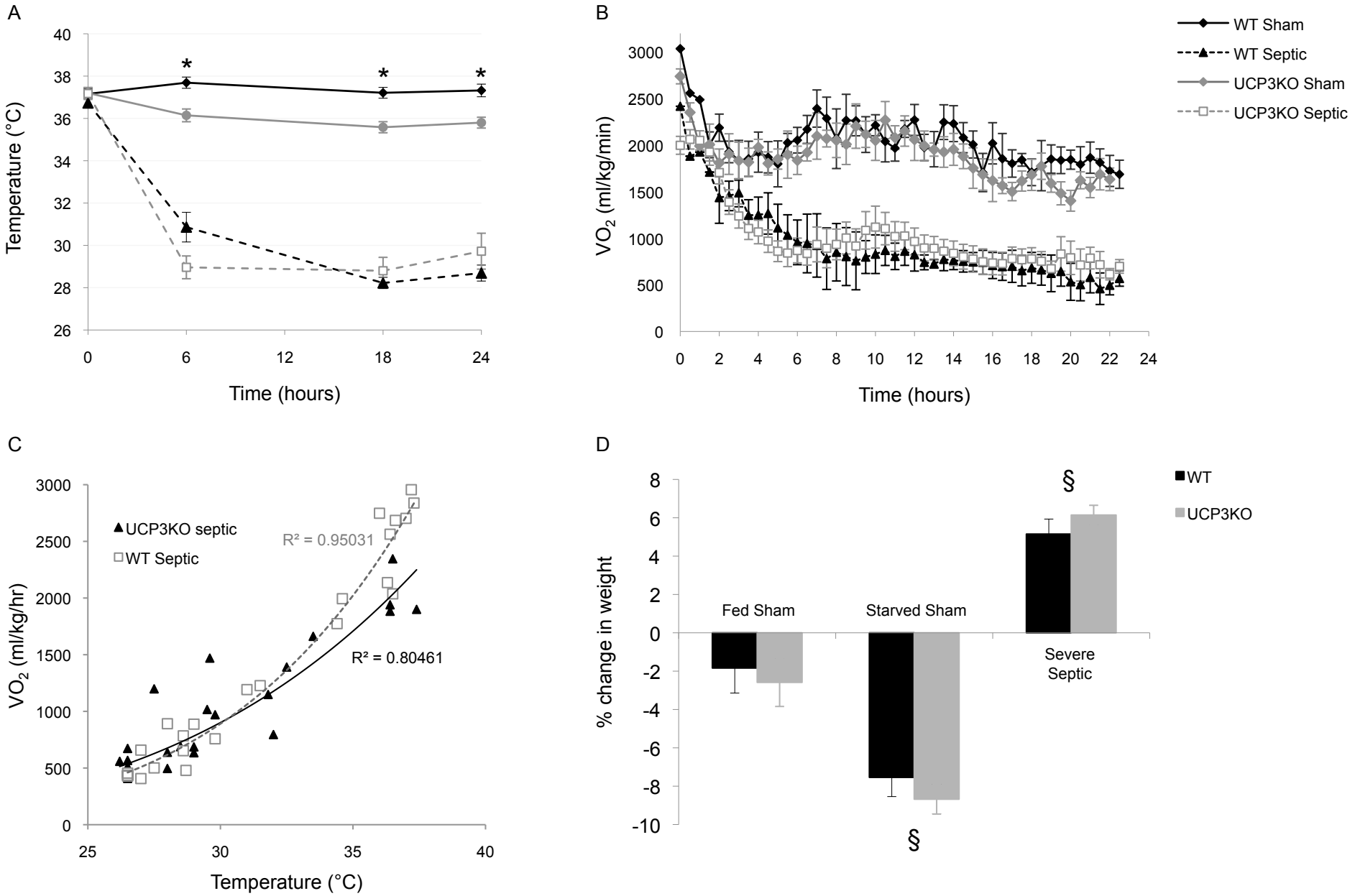
A
Temperature (°C)
Time (hours)
*
*
*
B
VO_2 (ml/kg/min)
Time (hours)
WT Sham
WT Septic
UCP3KO Sham
UCP3KO Septic
C
VO_2 (ml/kg/hr)
Temperature (°C)
UCP3KO septic
WT Septic
R² = 0.95031
R² = 0.80461
D
% change in weight
WT
UCP3KO
Fed Sham
Starved Sham
Severe Septic
§
§

Figure 4

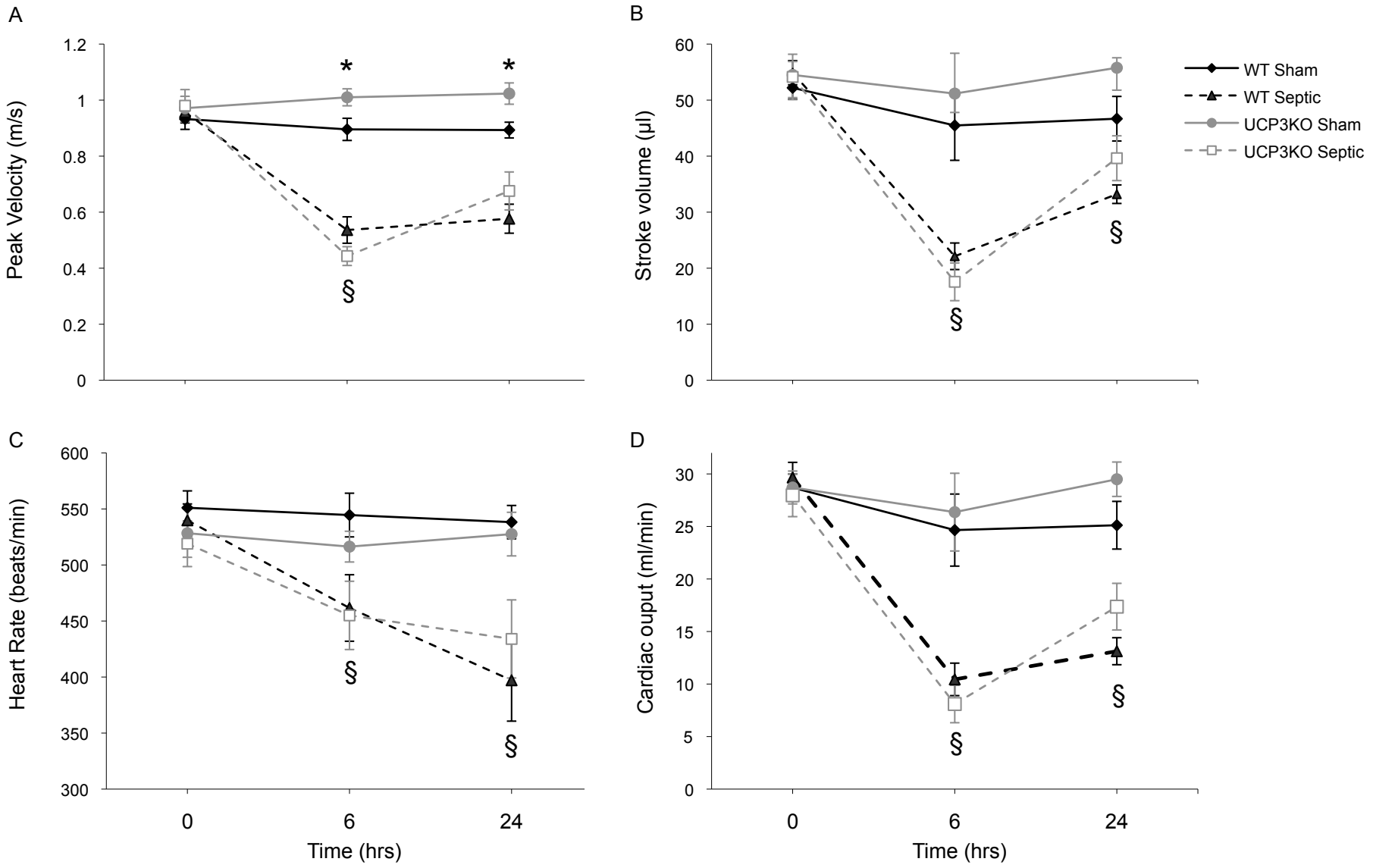
A
Peak Velocity (m/s)
1.2
1
0.8
0.6
0.4
0.2
0
*
*
§
B
Stroke volume (µl)
60
50
40
30
20
10
0
§
§
WT Sham
WT Septic
UCP3KO Sham
UCP3KO Septic
C
Heart Rate (beats/min)
600
550
500
450
400
350
300
§
§
0
6
24
Time (hrs)
D
Cardiac ouput (ml/min)
30
25
20
15
10
5
0
§
§
0
6
24
Time (hrs)

Fig 5

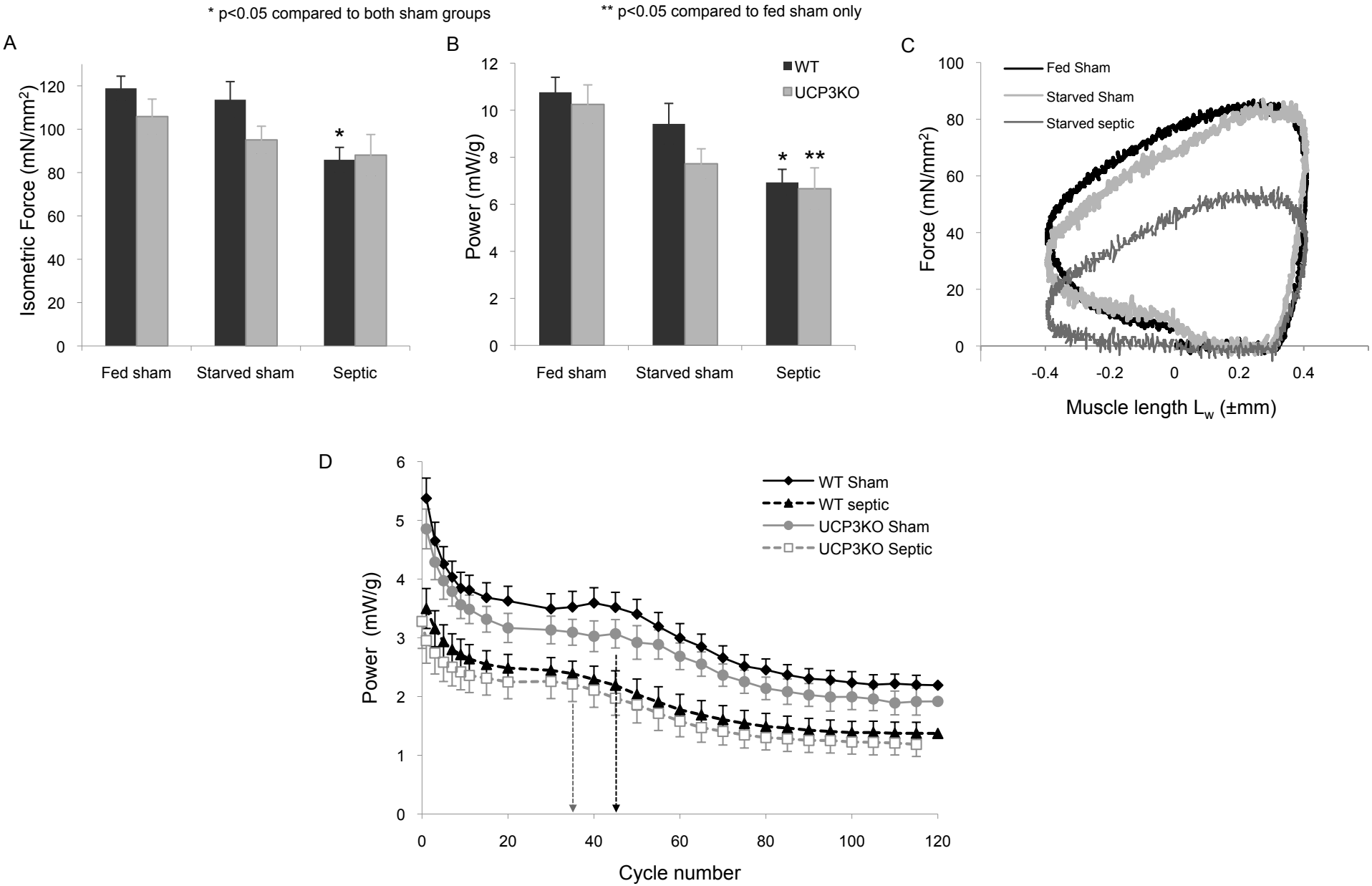
* p<0.05 compared to both sham groups
** p<0.05 compared to fed sham only
A
Isometric Force (mN/mm²)
Fed sham
Starved sham
Septic
B
Power (mW/g)
WT
UCP3KO
C
Force (mN/mm²)
Fed Sham
Starved Sham
Starved septic
Muscle length Lw (±mm)
D
Power (mW/g)
WT Sham
WT septic
UCP3KO Sham
UCP3KO Septic
Cycle number

Figure 6

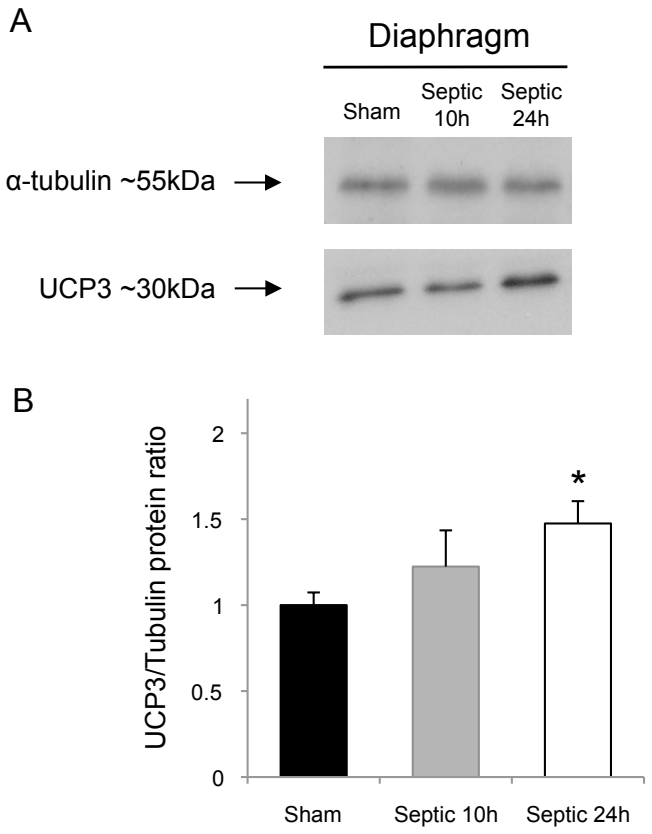
A
Diaphragm
Sham
Septic 10h
Septic 24h
α-tubulin ~55kDa
UCP3 ~30kDa
B
UCP3/Tubulin protein ratio
2
1.5
1
0.5
0
*
Sham
Septic 10h
Septic 24h

Figure 7

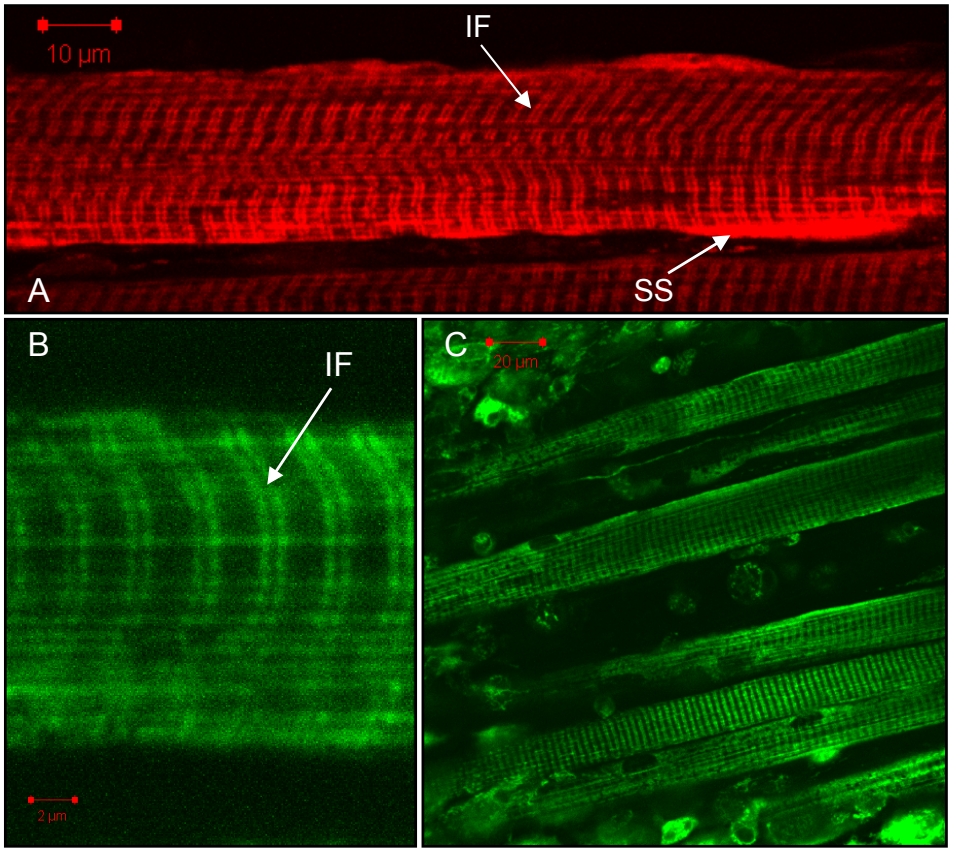
10 µm
IF
SS
A
B
IF
2 µm
C
20 µm

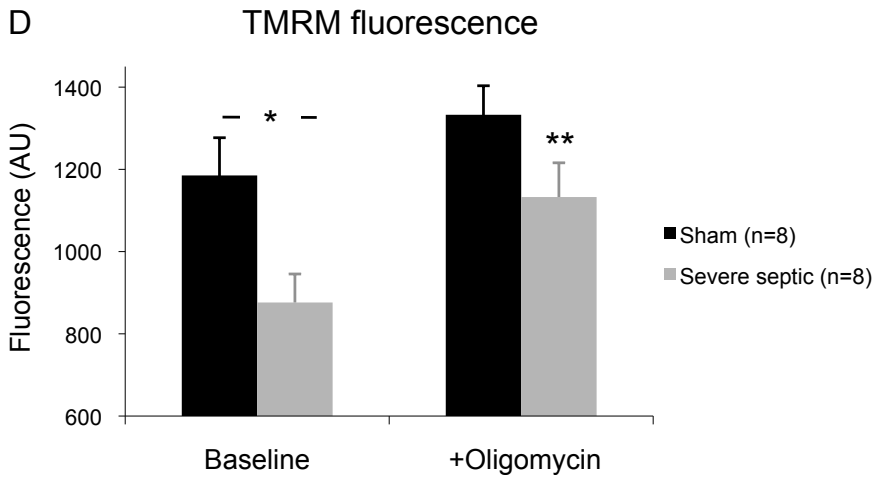
D
TMRM fluorescence
Fluorescence (AU)
1400
1200
1000
800
600
*
**
Baseline
+Oligomycin
Sham (n=8)
Severe septic (n=8)

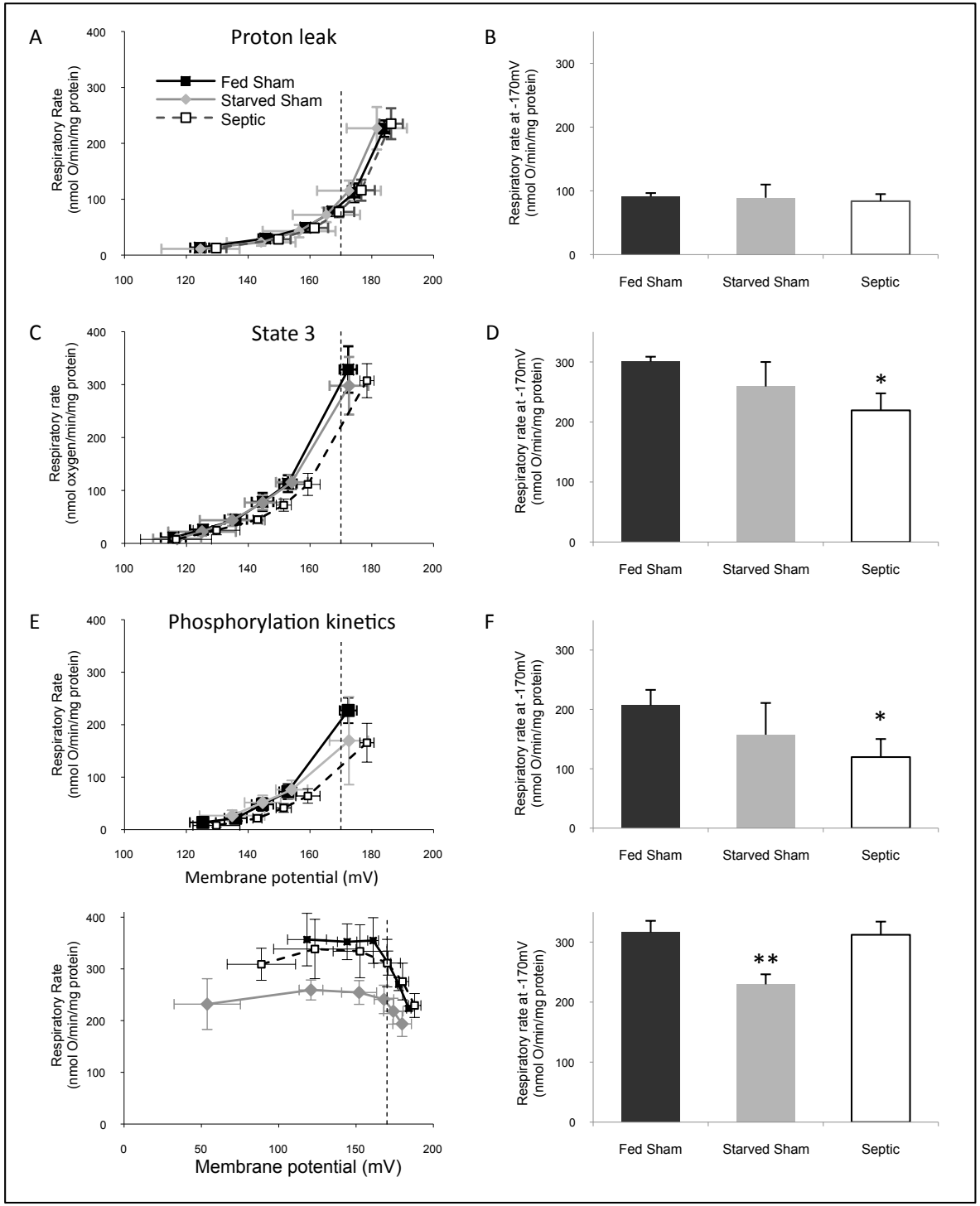
A
Proton leak
Fed Sham
Starved Sham
Septic
Respiratory Rate
(nmol O/min/mg protein)
B
Respiratory rate at -170mV
(nmol O/min/mg protein)
Fed Sham
Starved Sham
Septic
C
State 3
Respiratory rate
(nmol oxygen/min/mg protein)
D
*
E
Phosphorylation kinetics
Membrane potential (mV)
F
**

Figure 8